Institute of Physics Publishing
doi:10.1088/1742-6596/34/1/109
Journal of Physics: Conference Series **34** (2006) 662–667
International MEMS Conference 2006

Initial Test Results from a 3-axis Vibrating Ring Gyroscope

B.J. Gallacher, J.A. Neasham, J.S. Burdess and A.J. Harris

INSAT University of Newcastle upon Tyne

NE1 7RU

B.J. Gallacher@ncl.ac.uk

Abstract. There are several application areas where the simultaneous measurement of rates of rotation about three mutually orthogonal axes is required. In this paper the principle features of a 3-axis vibrating ring gyroscope are described. The fabrication process for the gyroscope is presented and employs standard MEMS techniques. The modal properties for the ring are measured experimentally using laser vibrometry and electrostatic sensing and compared with the design predictions. In operation as a rate gyroscope it is necessary to excite the primary motion of the gyroscope and control is amplitude. As Q-factors of vibratory gyroscope are typically of the order 10^3-10^4 slight variations in environmental conditions will perturb the natural frequency of the primary mode significantly. To ensure the primary motion of the gyroscope is maintained with constant amplitude a control scheme employing both frequency tracking and amplitude control is required. An electronic control system using digital signal processing (DSP) has been developed to ensure excitation of the primary motion occurs at resonance with controlled amplitude. The control scheme employs an embedded processor to generate the drive frequency (via a D/A converter) and to monitor the primary vibration (via an A/D converter). Experimental results from the control scheme highlighting its effectiveness over conventional PLL approaches are presented.

1. Introduction

MEMS technologies have been used successfully in the production of low-cost rate gyroscopes. For vibrating gyroscopes, the sensitivity to applied rates of rotation may be significantly improved by ensuring that the primary and secondary modes of vibration are "tuned". For "tuned" gyroscopes the natural frequencies of the driven mode, the primary, is near that of the sense mode, the secondary. Due to the axial symmetry of rings the flexural modes of vibration exist in degenerate pairs. Such degeneracy has been exploited in manufacturing single axis ring gyroscopes [1-4]. It has been shown [5,6] that ring designs may be developed further such that measurements of rate of rotation can be made about three mutually orthogonal axes.

In this paper the principles of the three axis ring gyroscope are described. The fabrication process used to produce prototype devices is outlined. The digital signal processing control used to ensure excitation occurs at resonance is also described. Experimental results obtained from the DSP control scheme are also presented.

2. Principles of Operation

The principal features of the design are the axi-symmetry of the ring sensing element and the cyclic-symmetric arrangement of the ligaments that connect the ring to the supporting casing. These features allow important natural frequencies of vibration of the ideal structure to exist in pairs [5,6], with the frequencies of the modes in each pair being identical. In such a case the modes of vibration are referred to as being degenerate. Thus the sensitivity to applied rates of rotation can be improved by matching the natural frequencies of those modal responses associated with rate measurement [5,6]. If this matching is not preserved, three axis measurements are still possible but the sensitivity of the sensing element to applied rates of turn is noticeably reduced.

Figure (1) illustrates the centre line of the ring. Reference axes OXYZ are fixed to the supporting casing and it is assumed that OZ is perpendicular to the plane containing the structure, with O at the centre of the ring. It is assumed that these axes rotate with an angular velocity $\underline{\Omega}=(\Omega_x, \Omega_y, \Omega_z)$. Motion of the ring relative to OXYZ is represented by the displacement, $\underline{r}$, of a typical point P on its centre line. This displacement is measured with respect to the local polar coordinate axes at P and is expressed by $\underline{r}=(u,v,w)^T$, where u, v and w are the radial, tangential and axial components, respectively. When operated as a gyroscope, a natural in-plane mode of the ring will be driven with constant amplitude of vibration at its natural frequency, ω_1. This motion, which is referred to as the primary motion of the gyroscope, is characterised by radial, u, and tangential, v, displacements having spatial variations of the form cosnϕ and sinnϕ respectively, where n is the mode number.

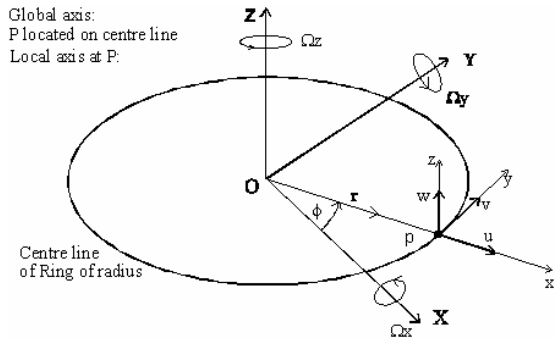

Figure (1) Coordinate System

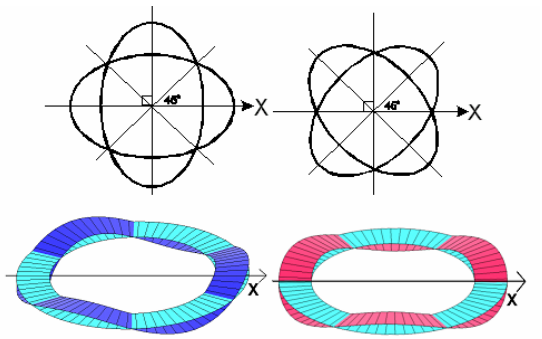

Figure (2) Modes of Vibration

A secondary in-plane mode of vibration of natural frequency ω_2 is excited due to Coriolis inertial forces produced as a result of the rate of rotation Ω_z, applied about the polar axis of the ring. For the perfectly formed ring with appropriate cyclic arrangement of the suspension $\omega_1=\omega_2$. Figure (2) shows the extreme modal displacement corresponding to the radial motion of the primary and secondary motions for the case n=2. For the applied rates of rotation Ω_x and Ω_y, the Coriolis inertial forces are directed out of the plane of the ring and excite the secondary modes characterized by axial displacements having natural frequencies ω_3 and ω_4 and spatial variations of the form $sin(m\phi)$ and $cos(m\phi)$, respectively, where $m = n \pm 1$. The design makes use of the case where $m=n+1$ and for the ideal ring with appropriate cyclic arrangement of the suspension $\omega_3=\omega_4$. Figure (2) shows the extreme modal displacement corresponding to the axial motion of the secondary modes for the case m=3.

The axial symmetry of the structure of the gyroscope ensures that both in-plane and out of plane flexural modes are degenerate and thus $\omega_1=\omega_2$ and $\omega_3=\omega_4$. However, in general $\omega_1 \neq \omega_3$ and the width and thickness must be chosen appropriately in order to result in the condition $\omega_1 \approx \omega_3$. In this case the gyroscope is "tuned for all four modes. A deliberate mis-tuning of 500 Hz between the in-plane and out of plane modes was introduced into the design. An electrostatic tuning scheme will be used to

reduce the natural frequencies of the out of plane modes towards that of the in-plane modes and thus establish tuning. The equation of motion of the gyroscope and also the natural frequencies have been obtained using a Lagrangian method. The details of the derivation are provided in [5].

3. Design

The critical dimensions of the gyroscope are shown in table (1). The parameters h_o and z_o are in-plane and out of plane capacitive gaps, respectively. The design dimensions are chosen such that the natural frequencies of the important modes of vibration are approximately 20 kHz.

gyroscope dimenions	
a	4mm
b	175μm
d	100μm
h_o	5μm
z_o	5μm

Table (1) Critical Dimensions

4. Fabrication Process

Crystalline silicon with its high intrinsic Q factor, stable material properties and well established processing techniques is a material already used heavily in the manufacturing of MEMs devices. Generally, crystalline silicon possesses anisotropic material properties. In order for the flexural modes of vibration of perfect circular rings to occur in degenerate pairs, the material properties of the ring must be isotropic. However, by using the appropriate crystal orientation, this anisotropy may be minimised. It may be shown [6] that if the cross-sectional dimensions of the ring are small in comparison with its radius then the effect of transverse shear on the natural frequencies will be small and thus (111) silicon will be isotropic.

The fabrication process makes use of DRIE of silicon, wet-etching of Pyrex and anodic bonding to form the 3-axis gyroscope. The fabrication process commences by first wet-etching Pyrex glass substrate in order to form a recess to allow out of plane vibration of the ring structure and also to form capacitive electrodes that are positioned below the ring structure to detect the out of plane vibration. The electrode regions are metalised using evaporated Ti/Au. The processed Pyrex substrates are then anodically bonded to double-side-polished (111) silicon substrates. The ring structure and also the capacitive in-plane electrodes are formed by DRIE. Figure (3) shows a portion of a gyro die and also the DRIE silicon layer of the gyro die.

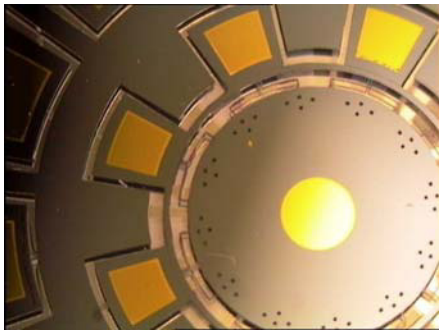

Figure (3a) Portion of Gyro Die

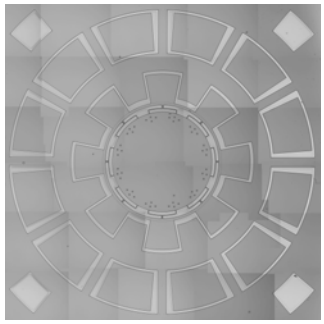

Figure (3b) Silicon Layer of Gyro Die

5. Modal Analysis Experimental Results

The modal properties of the out of plane modes of vibration were determined using laser vibrometry. This techniques permits the modeshapes of the out of plane modes to be measured and compared with the modeshapes of the perfect unsupported ring which have been used in the analytical model. By plotting the normalised magnitude of the out of plane displacement of the ring as a function of angular position, the perturbation of the measured modeshapes of the m=3 modes from the assumed $cos(m\phi)$ and $sin(m\phi)$ form of the perfect ring may be investigated. Figure (4) illustrates one of the measured m=3 modeshapes.

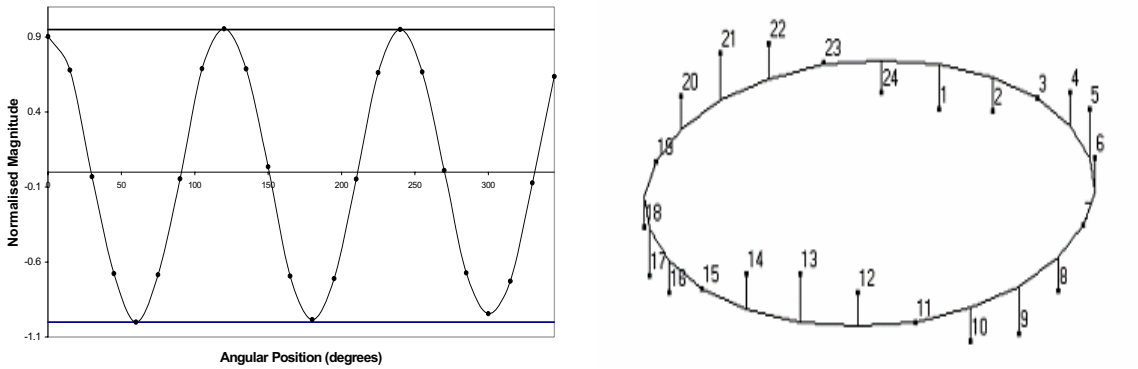

Figure (4) Measured Perturbation of m=3 Modeshape

The percentage difference between the maximum and minimum amplitudes gives a measure of the modeshape perturbation. From Figure (4) the perturbation of the modeshape has the value of 6%. The m=3 modeshape of the ideal suspended ring was calculated by the finite element model and was calculated to be perturbed by 0.04% from that of a perfect unsupported ring for a ligament width of the suspension of 20 μm. This increased perturbation may be attributed to variations in the ligament width and thickness increasing the out of plane stiffness of the suspension.

Figure (5) shows the frequency responses of the both out of plane modes of order m=3, measured using laser vibrometry and also the in-plane modes of order n=2, measured electrically. Table (2) summaries the results. All dynamic measurement were performed under vacuum at a pressure of 0.04 mbar. The Q-factor of the modes is ≈3000 thus the frequency split between modes within each pair is approximately equal to the bandwidth of each mode and may be reduced further by employing trimming procedures [7,8].

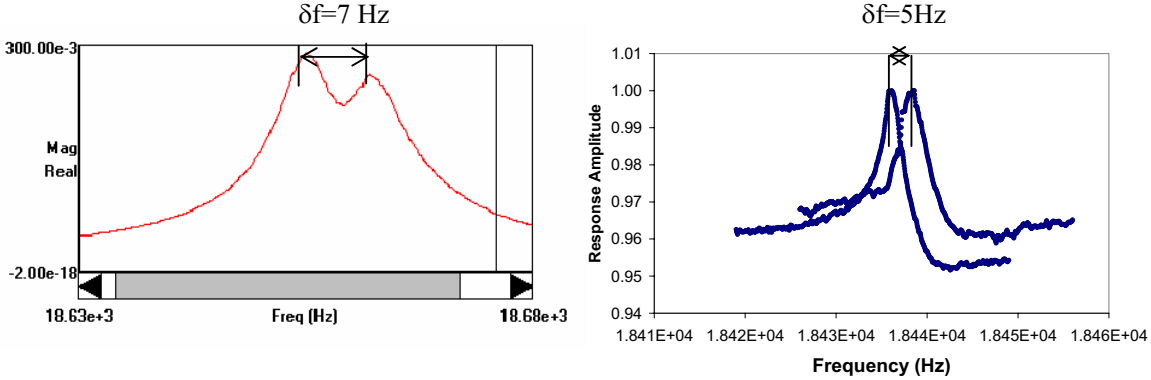

Figure (5) Measured Frequency Responses

	mode1	mode2	mode3	mode4	split 2-1	split 4-3	split 4-1
measured	18.438	18.434	18.650	18.657	-0.005	0.007	0.219
F.E.model	18.24	18.24	18.74	18.74			0.5
analytical Model	17.09	17.09	19.45	19.45			

Units: kHz

Table (2) Modal Analysis Results

6. Frequency Tracking and Amplitude Control

It is critical that the frequency of the primary mode excitation signal is controlled to maintain operation at the primary mode's natural frequency, thus minimising the influence of noise and capacitive feed-through. It is also important that the amplitude of the primary mode vibration is held constant to avoid any modulation of the secondary mode measurements. In previous work on vibratory MEMS devices, analog circuits based around the phase locked loop (PLL) and amplitude locked loop (ALL) were investigated to control the frequency and amplitude of the primary mode excitation respectively. This proved highly unsatisfactory due to dependence on the gain and phase response of the analog sensing circuits, capacitive feed-through effects and component tolerances. During this work, digital signal processing (DSP) techniques were employed to construct a novel control scheme with significant advantages in terms of accuracy, repeatability and flexibility.

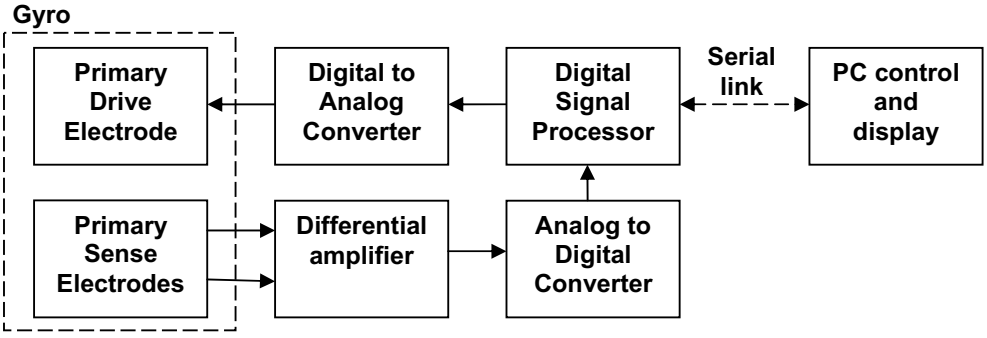

Fig.5 DSP based control system for primary excitation

Figure 5 illustrates the hardware components of the DSP control system. A floating point DSP, of the Analog Devices SHARC® family, is used to generate a sinusoidal drive signal via a digital to analog converter with 16 bit precision and a sampling rate of 48kHz. Due to the floating point arithmetic used, the frequency synthesis has practically unlimited resolution. The primary mode vibration is then detected electrostatically by a pair of electrodes, arranged in anti-phase, which are connected to a differential amplifier circuit. By adjustment of the relative gain applied to each sense electrode, the differential amplifier rejects the vast majority of the common mode signal arising from capacitive feed-through of the drive signal. The amplified primary sense signal is then digitised using an analog to digital converter, again with 16 bit precision and 48kHz sampling rate, for processing by the DSP. Additional analog input channels are also provided for processing of the secondary mode sense signals. A serial data link is provided to enable data to be displayed on a PC or operating parameters to be changed. Within the DSP, the primary sense signal is fed through a quadrature mixer with the same frequency synthesiser source as the primary drive. The output is then integrated over 960 samples and the magnitude calculated, achieving a perfectly coherent amplitude detector with a bandwidth of only 50Hz. This results in very high SNR on the detected signals.

On power up, the frequency acquisition and tracking algorithm starts by performing a wide bandwidth sweep and looking for the maximum vibration amplitude. This obtains a "first cut" estimate

of the resonant frequency as illustrated by figure 6(a). The frequency range and resolution is programmable but, for example, a 400Hz sweep with 4Hz resolution takes 2s to complete. Next a narrow band sweep is performed to lock onto the exact resonant frequency as shown in figure 6(b). Subsequent tracking to maintain the frequency lock is then achieved in one of two ways: narrow band sweeps can be repeated at programmable intervals (depending on the expected rate of drift) or frequency adjustments are automatically made when the vibration amplitude falls outside a programmable tolerance range. After each frequency lock or adjustment, the DSP can automatically adjust the drive signal amplitude to maintain the desired primary vibration amplitude. In addition, since the DSP is also processing the secondary sense signals, each measurement made can be normalised with the primary amplitude at an update rate of 50Hz to eliminate any amplitude drift.

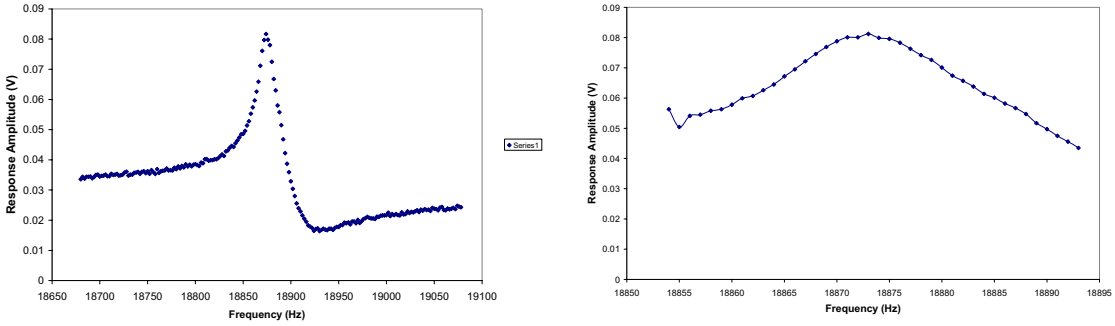

(a) (b)

Fig.6 DSP Tracking of Resonant Frequency: (a) wide band= 400 Hz, (b) narrow band=40Hz

Initial results suggest that DSP based excitation control and sense signal processing can deliver significant performance gains in vibrating ring gyroscopes and other MEMS devices. Furthermore the software/firmware solution leads to huge improvements in repeatability, compared to analog solutions, and easily adjustable operation from the same circuit. Future work will attempt to use this approach on higher frequency vibrational devices and to design a low cost, miniaturized, programmable logic based implementation that could be incorporated on a die or hybrid alongside the MEMS structure.

References

[1] Putty M W and Najafi K 1994 A micromachined vibrating ring gyroscope *Solid-State Sensor and Actuator Workshop*, Hilton Head pp 213-20.

[2] Pearce C H 2001 The performance and future development of a MEMS SiVSG and its application to the SiIMU *Symp. Gyro Technology* Stuttgart pp 6.0-6.10.

[3] Ayazi F and Najafi K 2001 A HARPSS polysilicon vibrating ring gyroscope *Journal of Microelectromechanical Systems* **10** 169-79.

[4] Harris A J, Burdess J S, Wood D, Langford R, Williams G, Ward M C L and McNie, M E 1998 Issues Associated With The Design, Fabrication and Testing of a Crystalline Silicon Ring Gyroscope With Electromagnetic Actuation and Sensing *Journal of Micromechanics and Microengineering* **8** 284-292.

[5] Gallacher B J, Burdess J S, Harris A J and McNie M E 2001 The principles of a multi-axis vibrating gyroscope *IEEE Trans. Aerospace and Electronic Systems* **37** 1333-43

[6] Gallacher B J 2002 The Design, Fabrication and Testing of a Multi-axis Vibrating Ring Gyroscope *Ph.D Dissertation* University of Newcastle upon Tyne

[7] Gallacher B J, Hedley J, Burdess J S, Harris A J and McNie M E 2003 Multi-Modal Tuning of a Ring Gyroscope using Laser Ablation, Journal of Mechanical Engineering Science-Part C **217** 557-576.